

Article

Comparing Photocatalytic Degradation of Gaseous Ethylbenzene Using N-doped and Pure TiO₂ Nano-Catalysts Coated on Glass Beads under Both UV and Visible Light Irradiation

Morteza Kamaei ^{1,2}, Hamid Rashedi ^{1,*}, Seyed Mohammad Mehdi Dastgheib ² and Saeideh Tasharofi ³

¹ School of Chemical Engineering, College of Engineering, University of Tehran, Tehran 1417614418, Iran; kamaei_morteza@yahoo.com

² Microbiology and Biotechnology Group, Environment and Biotechnology Research Division, Research Institute of Petroleum Industry, Tehran 1485733111, Iran; dastgheibsmm@ripi.ir

³ Ecology and Environmental Pollution Control Research Group, Environment and Biotechnology Research Division, Research Institute of Petroleum Industry, Tehran 1485733111, Iran; tasharofis@ripi.ir

* Correspondence: hrashedi@ut.ac.ir; Tel.: +98-216-111-3058

Received: 5 September 2018; Accepted: 4 October 2018; Published: 18 October 2018



Abstract: Volatile Organic Compounds (VOCs) are within the main industrial air pollutants whose release into the atmosphere is harmful to the ecosystem and human health. Gas-phase photocatalytic degradation of ethylbenzene, an aromatic VOC emitted from various sources, has been investigated in this study using TiO₂ nanoparticle-coated glass beads in an annular photoreactor. To use visible light irradiation, TiO₂ nanoparticles were doped by nitrogen using urea. The results showed that nitrogen doping significantly increased the removal efficiency of ethylbenzene under visible light irradiation compared with the pure TiO₂, so that the removal efficiencies between 75–100% could be yielded for the initial ethylbenzene concentrations up to 0.13 g/m³ under visible light which could be useful for improving indoor air quality. The UV irradiated reactor needed less residence time and much higher removal efficiencies could be yielded at high initial concentrations. When the residence time under UV irradiation was one third of the same under visible light, the removal efficiency was more than 80% for the inlet concentrations up to 0.6 g/m³, whereas the removal efficiency under visible light was about 25% at this inlet concentration. Langmuir-Hinshelwood kinetic model could be well fitted to the photocatalytic reaction in both irradiation systems.

Keywords: VOCs; ethylbenzene; Advanced Oxidation Process (AOP); photocatalysis; N-doped TiO₂; annular photoreactor

1. Introduction

Due to the development of industry within the last decades, environmental pollution has become a serious concern all over the world. In this regard, indoor and outdoor air contamination is a significant problem for the public health in both developing and developed countries [1,2]. Volatile organic compounds (VOCs), constituting a wide range of carbon-based materials, have been considered as major hazardous pollutants due to the fact that most of them are toxic and carcinogenic and can adversely affect both the human health and the ecological environment [3]. Among VOCs, monocyclic aromatic compounds such as ethylbenzene are widespread in the environment since they are emitted from various sources such as chemical and petrochemical plants as well as indoor sources including furnishings and office equipment which may be even a more important concern due to the fact that people spend most of their time in indoor environments [4,5].

Heterogeneous photocatalysis as an advanced oxidation process is a promising technology for abatement of such pollutants which has been the subject of attention in numerous research works in the last two decades and despite conventional treatment strategies including adsorption, absorption and condensation do not just transfer the treated compound from one phase to another one [6,7]. Gas-phase photocatalytic oxidation using semiconductor catalysts has a great potential in mineralization of pollutants and converting them to the harmless compounds such as water and carbon dioxide at room temperature and it is highly efficient at low concentration levels [8,9].

Titanium dioxide (TiO_2), a popular and highly effective semiconductor, has been extensively applied in photocatalytic oxidation processes owing to its distinguished features such as non-toxicity, low-cost availability, long-time photo-stability, as well as potent oxidizing power [10,11]. Degussa P-25, the commercial available form of TiO_2 nanoparticles, has been identified as the superior standard catalyst considering its high activity in heterogeneous photocatalysis for environmental applications due to having mixed phases of anatase and rutile and also its nano-sized structure [12]. The intrinsic restriction of TiO_2 is the lack of activity in visible light due to its relatively large band gap (about 3.2 eV). It requires ultraviolet (UV) light irradiation in order to produce electron-hole pairs that in the presence of oxygen or water can generate oxidizing agents including superoxide and hydroxyl radicals capable to degrade the target compounds [13,14]. Inducing photocatalytic activity of TiO_2 under visible light will lead to the hindrance of biohazardous and costly UV emissions and improve the feasibility of its application under the room lighting [8]. To prevail over the large band-gap energy, several methods including incorporating metal and non-metal elements as dopants into the TiO_2 lattice have been examined to enhance the photocatalytic activity under visible light irradiation. This treatment may also reduce the recombination of produced electron-hole pairs leading to a higher photocatalytic activity [15–17]. Nitrogen-doped TiO_2 , showing a remarkable red shift from the UV to the visible range, is one of the most extensively investigated anion-doped TiO_2 which serves as an outstanding visible light sensitive photocatalyst and also nitrogen is an eco-friendly element if increased in the environment by human pollution compared with some common metal dopants [18–20]. Moreover, in addition to the modification of TiO_2 nanoparticles as a pivotal necessity for increasing the photo-activity, the photoreactor is of high importance too [21]. There are several types of gas-phase laboratory scale photocatalytic reactors such as honeycomb monolith, annular, flat plate, packed-bed, membrane and optical fibre reactors, but generally an effective photoreactor should have a large specific surface area, small pass-through channels and direct irradiation to the reaction surface in order to provide appropriate contact among the reactants, catalysts and photons [22,23]. Among various proposed photoreactors, the annular packed-bed system can provide high surface area as well as efficient irradiation by installation of the light source at the center of the reactor [24].

For the specific investigated pollutant in this research work, gaseous ethylbenzene, there are some reports considering photocatalytic degradation with different catalysts. However, to the best of our knowledge, N-doped TiO_2 has not been already applied for photocatalytic degradation of ethylbenzene in the air. In addition, it should be noted that, in our research work, photocatalytic degradation has been conducted in continuous mode via catalysts coated glass beads providing an applicable photocatalytic system.

Therefore, considering the above-mentioned statements, in the present study the visible light photocatalytic degradation of gaseous ethylbenzene in the air has been investigated in an annular packed-bed photoreactor using N-doped Degussa P25 nanoparticles coated on glass beads and the removal efficiency of ethylbenzene under both UV and visible light irradiation using nitrogen doped and pristine Degussa P25 catalysts was compared.

2. Results and Discussion

2.1. Characterization of Photocatalysts

X-ray diffraction (XRD) pattern of the prepared N-doped P25 nanoparticles is shown in Figure 1. As for the obtained peaks which are attributable to the reports of Joint Committee on Powder Diffraction Standards (JCPDS) card No. 21-1272 for anatase and JCPDS card No. 21-1276 for rutile [25,26], it contains both anatase and rutile phases with a domination of anatase just like the pristine Degussa P25 [26,27], and no remarkable phase transformation occurred due to the low calcination temperature (400 °C), as observed by others [26,28]. The crystallite average size calculated using the Scherrer equation was found to be about 40 nm, well comparable to the particles size obtained from field emission scanning electron microscope (FE-SEM) images.

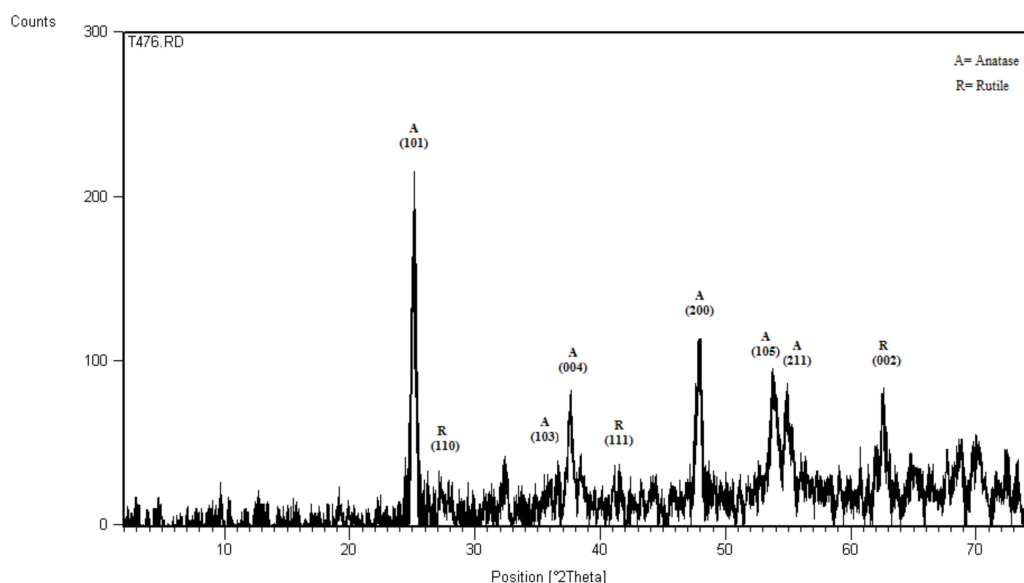


Figure 1. X-ray diffraction (XRD) pattern of the prepared N-doped TiO₂.

The specific surface area of the N-doped TiO₂ catalyst obtained by Brunauer-Emmett-Teller (BET) experiments was 53.32 m²·g⁻¹, close to the un-doped P25 BET surface area which had a value of 60.45 m²·g⁻¹ but showing a slight decrease, in agreement with other similar reports [28,29]. The average pore size of the prepared N-doped TiO₂ obtained by BET experiments was 15.25 nm which is considered to be mesopore based on the pore size categories recommended by International Union of Pure and Applied Chemistry (IUPAC) comprising micropores (d < 2 nm), mesopores (2–50 nm) and macropores (d > 50 nm) [17,30]. Nitrogen adsorption-desorption isotherms of the N-doped TiO₂ is shown in Figure 2. According to the shape of curve related to nitrogen isotherm plot, the as-prepared catalyst was type IV of the BDDT (Brunauer-Deming-Deming-Teller) classification with H3 hysteresis loop, demonstrating the presence of mesoporous material [31]. Also, the inset of Figure 2 indicates the pore size distribution determined by BJH (Barrett-Joyner-Halenda) method from the desorption branch of nitrogen isotherm. As showed in the related curve, the pore size distribution has a relatively wide range of about 3–100 nm with a maximum value around 15 nm, but most of the pore size is distributed in less than 50 nm representing the mesoporous material.

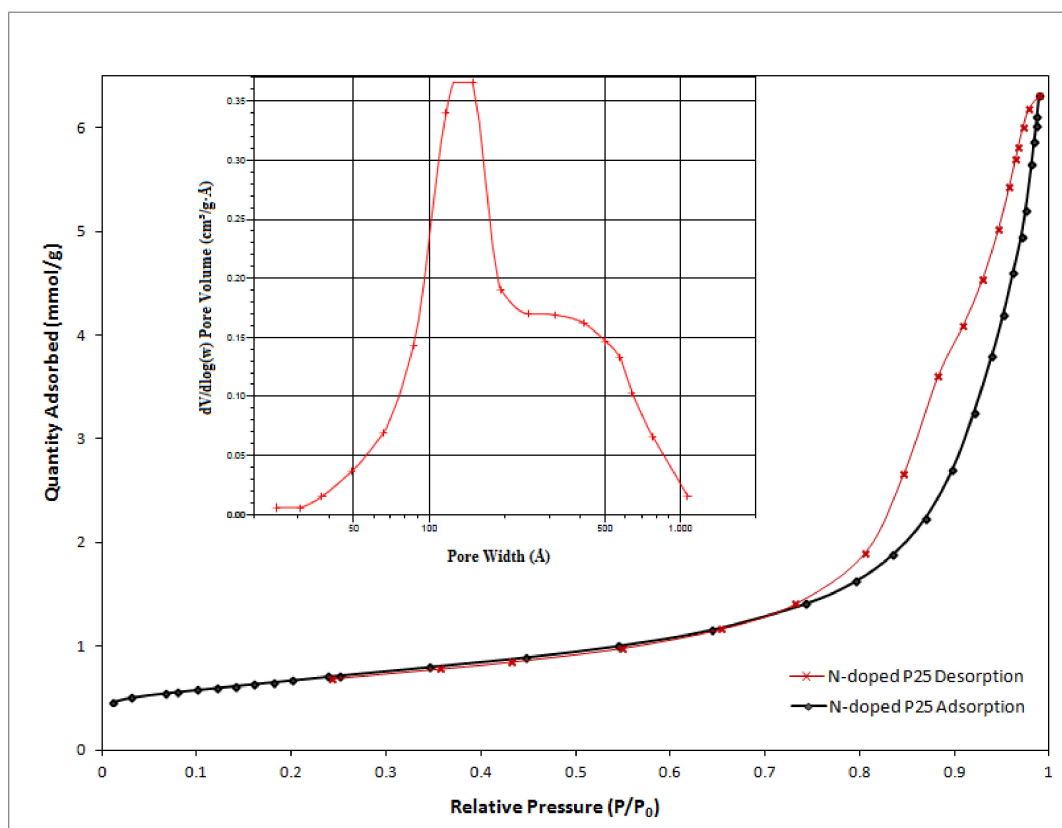


Figure 2. Nitrogen adsorption-desorption isotherms of as-prepared N-doped P25. The inset shows the Barrett-Joyner-Halenda (BJH) pore size distribution curve.

Figure 3 shows the FE-SEM images of the prepared N-doped TiO_2 catalysts. It can be seen that the prepared nanoparticles have a spherical morphology and their sizes are in the range of about 26–40 nm, which is well comparable to the average crystallite size obtained by the Scherrer equation (40 nm). Loose agglomeration could also be observed in the images.

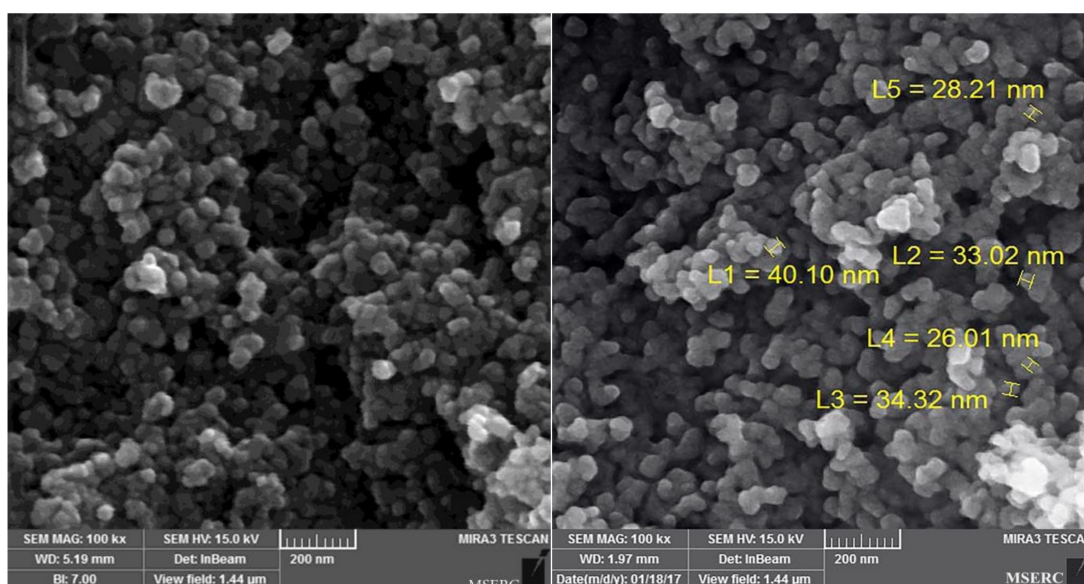


Figure 3. Field emission scanning electron microscope (FE-SEM) images of the as-prepared N-doped TiO_2 catalyst.

Moreover, the elemental composition of the as-prepared doped TiO_2 catalyst was determined by energy dispersive X-ray spectroscopy (EDS). The atomic percentage of nitrogen content obtained by EDS analysis was 7.1%. As shown in Figure 4, the EDS spectra obviously confirm the presence of Ti, O and N peaks which is an evidence of achieving N-doped TiO_2 catalyst.

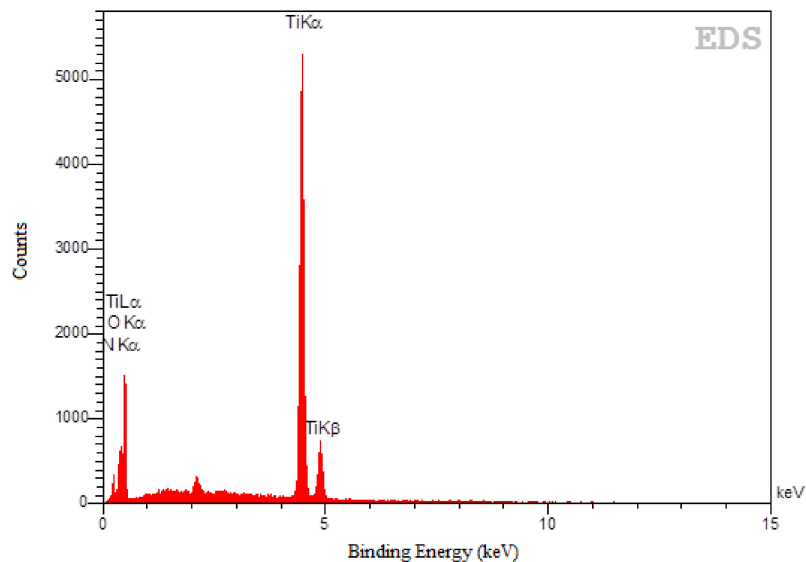


Figure 4. Energy dispersive X-ray spectroscopy (EDS) pattern of the as-prepared N-doped TiO_2 catalyst.

Furthermore, the FE-SEM images of the surface of roughened uncoated glass beads in different magnitudes and the surface of the coated ones in the same magnitude beside each other are shown in Figure 5. As seen in the images of Figure 5a on the left side, the uncoated glass beads have a roughened surface with wrinkles and cracks. The images of coated glass beads in Figure 5b on the right side, obviously confirm the deposition of N-doped TiO_2 nanoparticles on their surface which in a proper zoom the spherical morphology of the prepared catalysts in agglomerated form could be seen on the surface of these coated glass beads, the same as the SEM images of prepared catalysts in Figure 3.

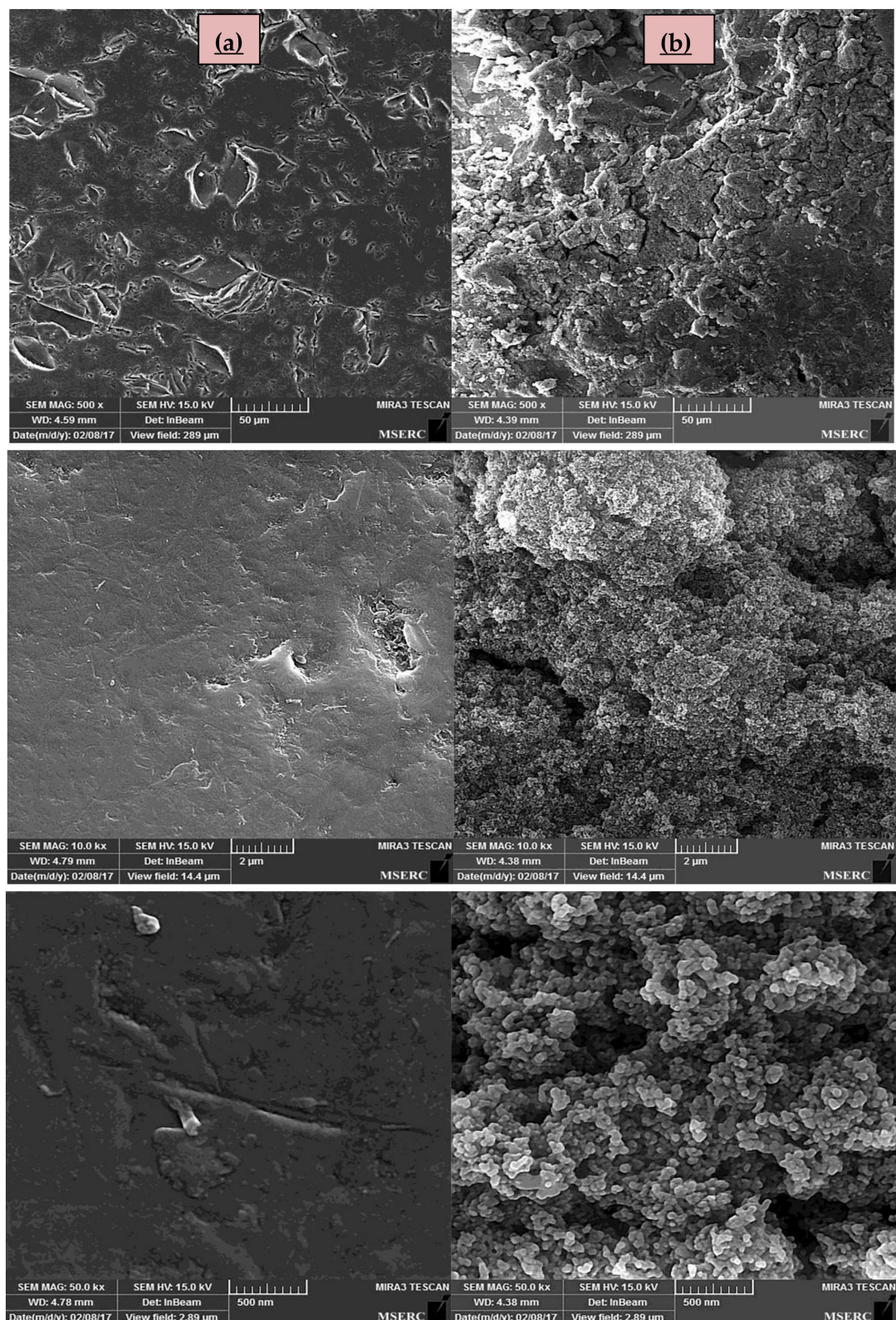


Figure 5. SEM images of the surface of (a) uncoated glass beads; (b) the glass beads coated by N-doped TiO₂ catalyst in different magnitudes.

Besides, the XPS analysis was performed to demonstrate nitrogen doping in the TiO₂ lattice and to investigate the chemical state of elements in the prepared N-doped TiO₂ catalyst. As shown in

Figure 6a, the XPS spectra of Ti2p indicates two peaks at binding energies of 458.3 eV and 464.3 eV confirming the presence of Ti2p_{3/2} and Ti2p_{1/2} which are the typical characteristics of Ti⁴⁺ oxidation state [32]. Figure 6b exhibits the XPS spectra of O1s region. The major O1s peak at the binding energy of 529.7 is originated from the Ti–O bonds in the TiO₂ lattice and the middle peak at binding energy of 530.9 eV could be attributed to titanium oxynitride phase, while the other minor peak at 532.8 eV can be assigned to the surface adventitious species such as oxygen in carbonate, hydroxides and water adsorbed on the catalyst surface during the sample characterization [18,33]. The deconvolution of N1s region in Figure 6c indicated two peaks at the binding energies of 399.1 eV and 401.7 eV which the first one at 399.1 eV could be ascribed to the N atoms located at the interstitial sites of the TiO₂ lattice as the Ti–O–N and/or Ti–N–O bonds [19,34,35] and the peak at 401.7 eV could be attributed to the nitrogen atoms that molecularly chemisorbed on the sample [18,33]. The atomic percentage of nitrogen content obtained by XPS analysis was 5.6%. The XPS spectra of C1s region is shown in Figure 6d. The sharp photoelectron peak at 284.8 eV is attributed to adventitious carbon due to sample contamination and the very weak peak at 288.5 eV can be assigned to the presence of carbonates on TiO₂ surface formed during the thermal decomposition of urea [29,33]. Therefore according to the XPS results, nitrogen incorporated into the TiO₂ lattice as the form of interstitial nitrogen doping along with the molecular chemisorption.

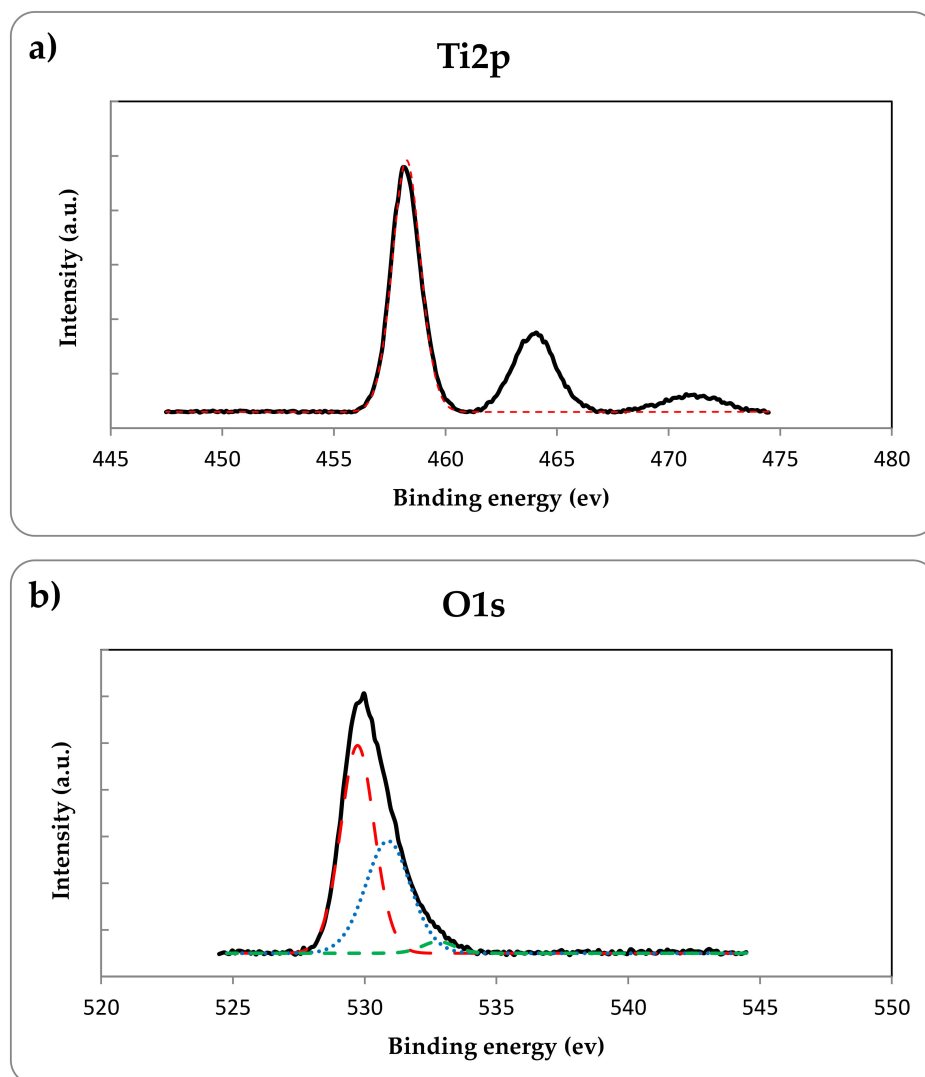


Figure 6. Cont.

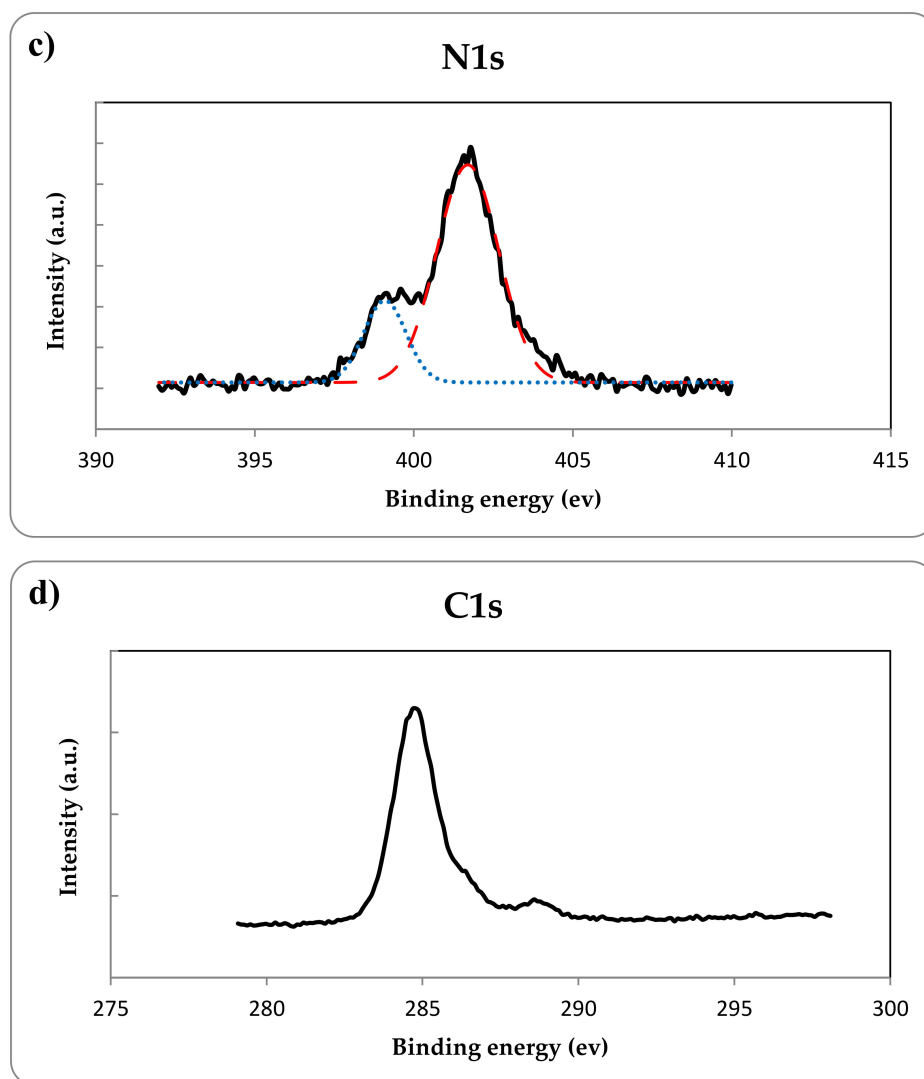


Figure 6. XPS spectra of (a) Ti2p, (b) O1s, (c) N1s and (d) C1s for the prepared N-doped TiO₂. The colored dashed lines stand for the deconvoluted scan of the elements which show all the obtained peaks for each element.

The UV-Vis diffuse reflectance spectra (DRS) of a photocatalyst play a key role in understanding its photocatalytic properties. The UV-Vis absorption spectra of the as-prepared N-doped TiO₂ and the pristine P25-TiO₂ catalysts obtained by the DRS test are shown in Figure 7a. The prepared N-doped TiO₂ catalyst exhibited an improved light absorption in both UV and visible regions compared with the pure P25-TiO₂ catalyst which had much less absorption in the visible region as expected and a red shift of absorption edge could be observed for the N-doped catalyst. Furthermore, the Kubelka-Munk function ($F(R)$) with indirect transition was applied in order to estimate the band gap energy of the samples due to considering TiO₂ as an indirect semiconductor [10,31]. The band gap energies were obtained by the intersection between the tangent line of the related curves and the photon energy ($h\nu$) axis in the plot of $(F(R) \times h\nu)^{0.5}$ against the energy of light (Figure 7b). The band gap energy of the N-doped TiO₂ had a value of about 2.9 eV, lower than the value of about 3.12 eV obtained for the pristine P25-TiO₂. Due to the mentioned evidence, doping TiO₂ with nitrogen resulted in enhancement of the visible light absorption and also reduction of the band gap energy and the as-prepared N-doped TiO₂ is anticipated to be visible light responsive.

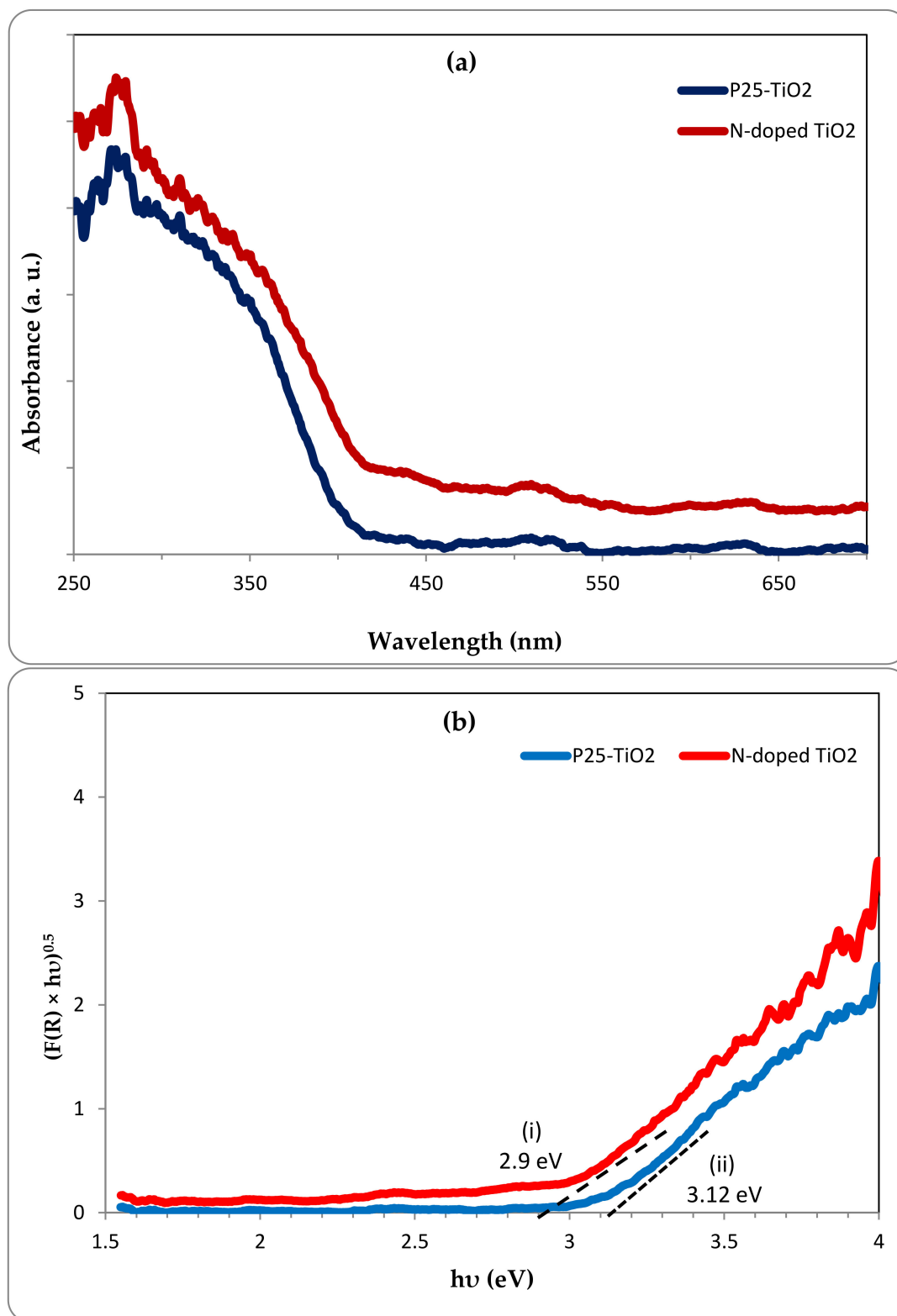


Figure 7. (a) UV-Vis diffuse reflectance spectra and, (b) plots of the transformed Kubelka-Munk function vs the photon energy for N-doped TiO₂ and pristine P25-TiO₂.

2.2. Photocatalytic Degradation Tests

The photocatalytic degradation of ethylbenzene in the air was evaluated in the mentioned photoreactor using the as-prepared N-doped TiO₂ and commercial TiO₂ under both UV and visible

light irradiation. Before starting the photocatalysis of ethylbenzene, some control experiments were performed under UV irradiation in the photoreactor packed with uncoated glass beads. Ethylbenzene degradation under UV irradiation without photocatalyst in the reactor was less than 2% even in relatively long residence time and low concentration. Therefore, ethylbenzene conversion was caused mainly by photocatalysis and the photolysis of ethylbenzene in the photocatalytic system could be considered negligible.

The removal efficiency of ethylbenzene using N-doped TiO₂ and pristine P25-TiO₂ photocatalysts under UV irradiation in different inlet concentrations (about 0.2–1 g/m³) and the desired residence time of 1 min is shown in Figure 8. The feed flow rate was fixed at 230 mL/min. The removal efficiency at the residence time of 1 min was not affected by increase in the inlet concentration up to the concentration of about 0.4 g/m³ (about 100 ppmv) and showed an efficiency of 100% in ethylbenzene degradation, but for greater inlet concentrations the removal efficiency decreased continuously and reached to the value of 38% at inlet concentration equal to 1.085 g/m³ (250 ppmv) which could be due to insufficient sites for adsorption of active radicals that have been occupied by the extra ethylbenzene load entering the reactor which is in agreement with other similar reports [6,36]. For instance, Jeon et al. [36] investigated the photocatalytic decomposition of some VOCs by TiO₂ photocatalyst coated on perforated planes in a cylindrical UV reactor and observed that the removal efficiency of ethylbenzene 60% decreased by increasing the inlet concentration from 0.1 g/m³ to 0.6 g/m³ due to blocking more active sites on the catalyst surface. Also as demonstrated in Figure 8, there was not a significant difference between N-doped TiO₂ and pristine P25-TiO₂ in photocatalytic decomposition of ethylbenzene under UV irradiation and the improvement of photocatalytic degradation using N-doped catalyst under UV irradiation was less than 5% compared with the un-doped TiO₂ catalyst.

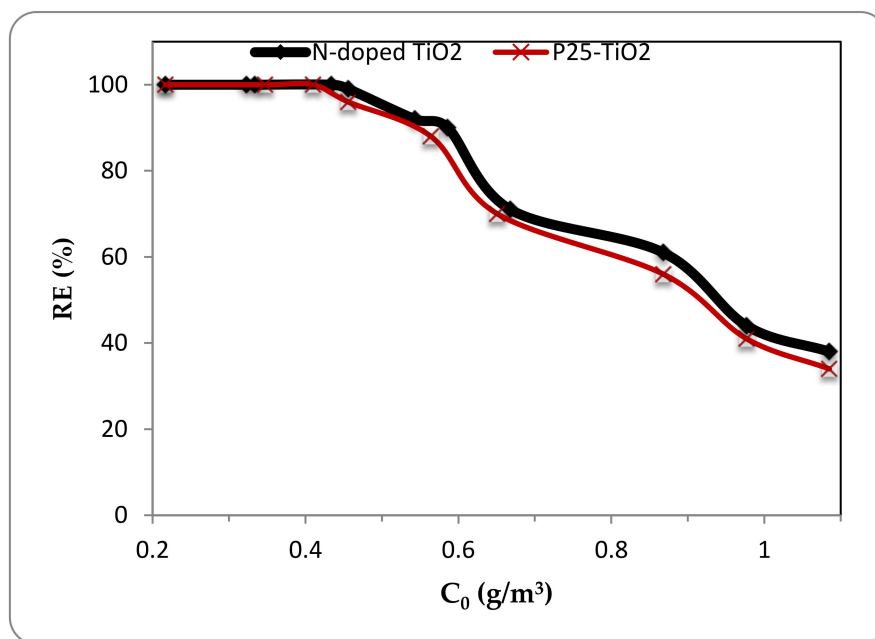


Figure 8. Effect of inlet concentration on removal efficiency at 1 min residence time under UV irradiation for N-doped and pristine TiO₂.

Despite UV irradiation, the photocatalytic reaction under visible light needed more residence time in the photoreactor for a proper degradation. The results showed that the photocatalytic activity under visible light could be achieved in longer residence times and lower inlet concentrations compared with the photocatalytic decomposition of ethylbenzene under UV radiation. Figure 9 indicates the removal efficiency of ethylbenzene under visible light irradiation at the residence time of 3 min using N-doped TiO₂ and pristine P25-TiO₂ photocatalysts in different inlet concentrations (about 0.03–0.6 g/m³).

The feed flow rate was fixed at 75 mL/min. The first point catching attention under visible light irradiation was the considerable different of ethylbenzene removal efficiency between N-doped and pristine TiO₂ catalysts despite the results obtained for UV radiation. As indicated in Figure 9, the N-doped photocatalyst had much better removal efficiency in different inlet concentrations under visible light and showed about three times higher removal efficiency compared with the un-doped TiO₂. However, in case of increasing inlet concentration effect in the fixed residence time of 3 min under visible light, similar behavior to UV irradiation was observed and the removal efficiency continuously declined insofar as the complete photocatalytic decomposition of ethylbenzene using N-doped TiO₂ for inlet concentration of 0.08 g/m³ (about 20 ppmv) decreased to the removal efficiency of 25% for inlet concentration of 0.6 g/m³ (about 140 ppmv).

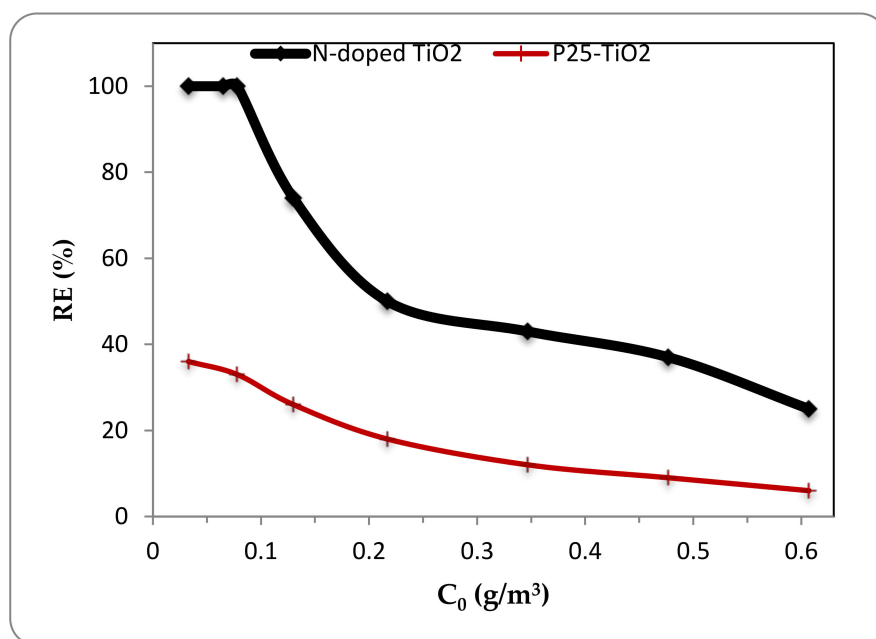


Figure 9. Effect of inlet concentration on removal efficiency at 3 min residence time under visible light irradiation for N-doped and pristine TiO₂.

Moreover, investigating the removal efficiency in different residence times demonstrated that the feed flow rate is a key parameter in photocatalytic performance under both UV and visible light irradiation. In other words, the flow rate was investigated via the residence time parameter. It should be noted that there is an inversely relation between residence time and the flow rate. Figure 10 indicates the removal efficiency of ethylbenzene using N-doped TiO₂ in different residence times under UV and visible light. The feed flow rates of 460 mL/min, 230 mL/min and 140 mL/min were applied to investigate the effect of three residence times of 30 s, 60 s and 100 s on the removal efficiency under UV irradiation. Also, the related values of flow rate under visible light irradiation were 115 mL/min, 75 mL/min and 30 mL/min respectively. The removal efficiency was significantly affected by the feed flow rate, since increasing the residence time in the reactor or in other words decreasing the feed flow rate resulted in enhancement of photocatalytic degradation under both UV and visible light radiation. This could be due to formation of more active radicals during the longer time that ethylbenzene molecules stay in photoreactor at lower inlet flow rates and enhancing the contact time between reactants and hydroxyl radicals. As exhibited in Figure 10, using the N-doped TiO₂ catalyst under UV irradiation and inlet concentration of 0.66 g/m³ (about 150 ppmv), the removal efficiency of 100% for residence time of 100 s decreased to the value of 26% at the residence time of 30 s. Also, under visible light irradiation and inlet concentration of 0.13 g/m³ (about 30 ppmv), increasing the residence time from 120 s to 420 s caused the removal efficiency to enhance from 36% to 97%. This is consistent with the work of Chun and Jo [37] who investigated photocatalytic decomposition of vaporous aromatics

including ethylbenzene in a plug-flow reactor under visible light using C-TiO₂ photocatalysts. They reported that when the flow rate became four times greater, the ethylbenzene degradation efficiency decreased from 100% to 38% due to insufficient mass transfer as a result of the short residence time [37].

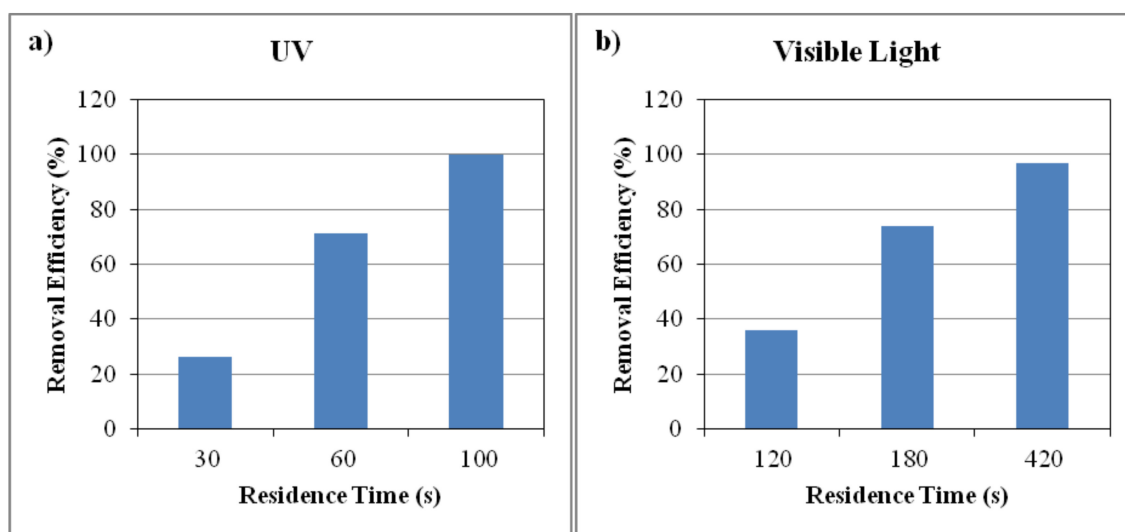


Figure 10. Ethylbenzene removal efficiency using N-doped TiO₂ under (a) UV irradiation and inlet concentration of 0.66 g/m³ at different residence times; (b) visible light and inlet concentration of 0.13 g/m³ at different residence times.

Besides, the carbon dioxide as a final product of VOCs photocatalytic reactions [13,18] was measured in the photoreactor. Figure 11 shows the CO₂ production by photocatalysis using N-doped TiO₂ catalysts against the ethylbenzene inlet load entering the reactor. The results showed that CO₂ production under UV irradiation was much higher than the visible light which is due to the considerable higher amount of ethylbenzene in the inlet flow of the reactor under UV radiation on one hand and also the greater capability of UV irradiation for photocatalytic conversion of such higher inlet concentrations on the other hand. As shown in Figure 11, increasing the ethylbenzene inlet load led to a continuous enhancement of CO₂ production to a maximum value, but further addition of ethylbenzene inlet load did not lead to CO₂ increase anymore and slightly reduced the CO₂ production in photoreactor which is in accordance with the obtained removal efficiencies at low and high inlet concentrations shown in Figures 8 and 9. The maximum value of CO₂ production under UV irradiation was about 1.6 g/m³·min in the investigated range of ethylbenzene inlet load (about 0.2–1 g/m³·min). Under the visible light radiation the amount of CO₂ reached to a maximum value of 0.16 g/m³·min in the investigated range of ethylbenzene inlet load (about 0.02–0.2 g/m³·min).

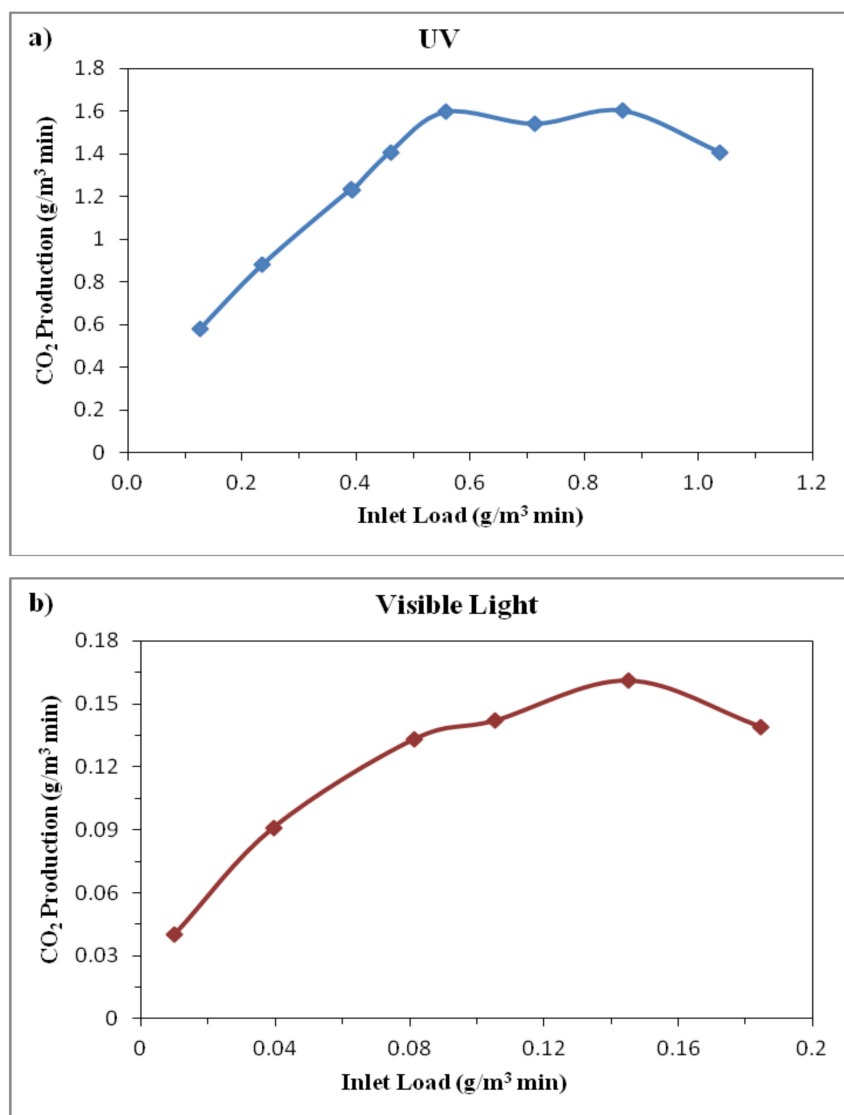


Figure 11. CO₂ production against the ethylbenzene inlet load in photocatalytic reactions using N-doped TiO₂ catalyst under (a) UV and (b) visible light irradiation.

2.3. Kinetic Analysis

Photocatalytic reaction rate in many cases could be generally described by the Langmuir-Hinshelwood (L-H) kinetic model providing a satisfactory presentation of the relationship between degradation rate and the initial concentration [6,15,21]:

$$r = (k_r KC)/(1 + KC), \quad (1)$$

where k_r is the L-H reaction rate constant, K is the reactant adsorption coefficient and C is the initial concentration of the reactant.

According to the above-mentioned equation, the reaction rate constant and adsorption coefficient could be achieved using the obtained experimental data for reaction rate and consequently plotting the inverse reaction rate versus the inverse initial concentration. Figure 12 shows the plot of $(1/r)$ versus $(1/C_0)$ for the experimental data obtained during the first 10 min of the reaction using N-doped TiO₂ catalyst in different concentrations and flow rates. As indicated in Figure 12, the related plots under both UV and visible light irradiation demonstrate appropriate fit to the Langmuir-Hinshelwood kinetic model. Furthermore, the reaction rate constant and adsorption coefficient calculated using the

slope and intercept of the obtained linear fit under UV radiation had the values of $0.889 \text{ g/m}^3 \cdot \text{min}$ and $1.26 \text{ m}^3/\text{g}$, respectively. The related values calculated under visible light irradiation were $0.085 \text{ g/m}^3 \cdot \text{min}$ for reaction rate constant and $4.69 \text{ m}^3/\text{g}$ for adsorption coefficient. The considerable difference between obtained results under UV and visible light irradiation is also obvious here for reaction rate constants and the one obtained for UV irradiation was much higher than the visible light as expected.

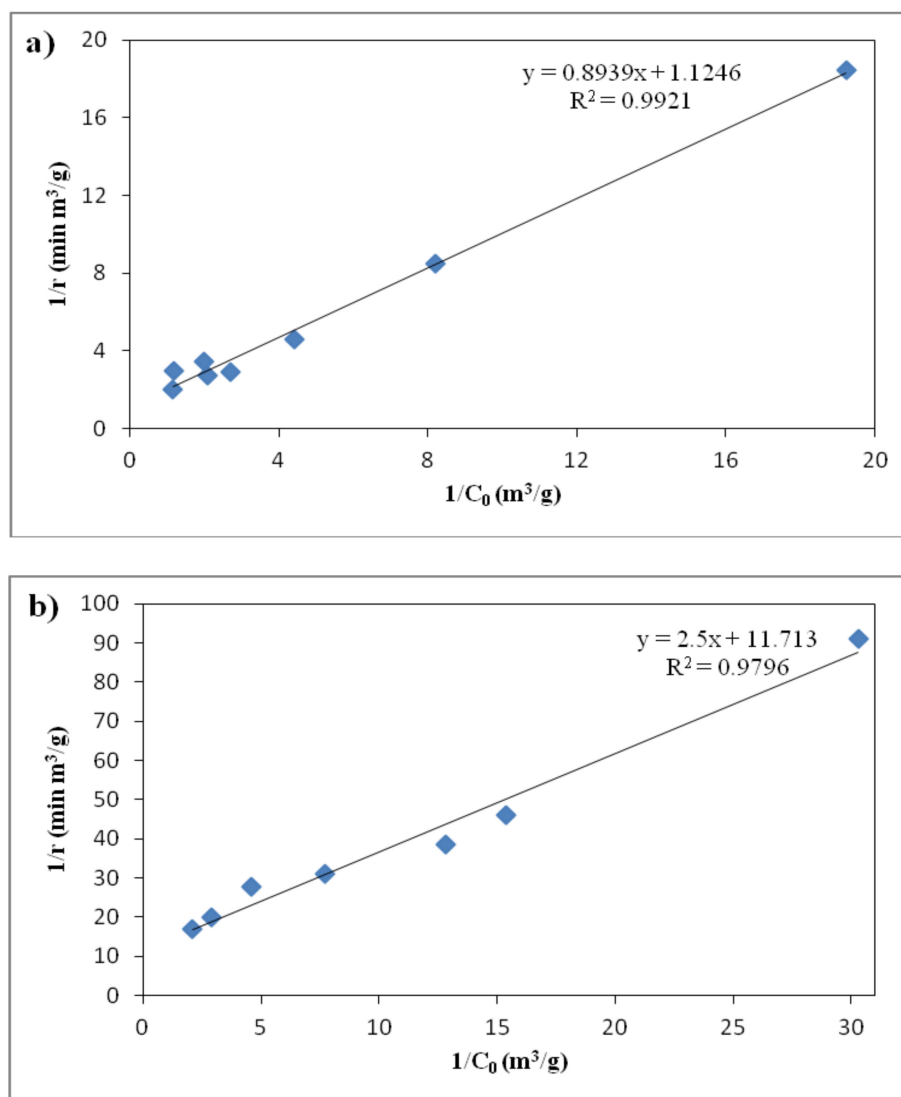


Figure 12. The relationship between the inverse of reaction rates and ethylbenzene initial concentrations using N-doped TiO_2 catalyst under (a) UV and (b) visible light irradiation.

The results for photocatalytic degradation of ethylbenzene obtained in this study are comparable with other similar works. Hinojosa-Reyes et al. investigated the decomposition of ethylbenzene in air stream using indium-doped TiO_2 photocatalysts immobilized on perlite granules in a plug-flow photoreactor with a concentric cylindrical configuration. They could obtain a maximum decomposition of 27.4% for ethylbenzene inlet concentration of 1.5 g/m^3 under 254 nm UV irradiation which is comparable to the removal efficiency of 38% for ethylbenzene inlet concentration of about 1.1 g/m^3 obtained in this research [38]. Also, lanthanum-doped TiO_2 nanotubes were used by Cheng et al. [6] in a continuous plug flow photoreactor for photocatalytic degradation of gaseous ethylbenzene under UV irradiation. Photocatalytic conversion of ethylbenzene decreased by increasing the initial concentration in their work similar to the results obtained here in this research but they achieved a photocatalytic

conversion of 58% for the initial concentration of 0.25 g/m^3 which was less than the 100% removal efficiency for the same initial concentration obtained here in this study. Although the residence time of 1 min in this study was higher than the same in their work which was about 20 s.

3. Materials and Methods

3.1. Photocatalyst Preparation

Degussa (Evonik) P25 nano-powder was used as the starting material to prepare the catalysts. N-doped TiO_2 was obtained using the mechanical mixing method and annealing described by Rengifo-Herrera et al [29]. TiO_2 (P25) and urea)as the nitrogen source(were mixed with a 4:1 ratio and grinded in a planetary ball mill (Retsch PM100; Retsch GmbH, Haan, Germany) for 1 h and then calcined under air atmosphere at $400 \text{ }^\circ\text{C}$ during 1 h with a heating rate of $10 \text{ }^\circ\text{C}$ per minute and cooled at room temperature. Afterwards, the obtained powder was washed three times with deionized water and dried at $70 \text{ }^\circ\text{C}$ and finally crushed in an agate mortar in order to achieve N-doped TiO_2 as a yellowish fine powder.

3.2. Characterization of Photocatalysts

The specific surface area of N-doped P25 was calculated by the BET method using nitrogen adsorption-desorption at 77 K via a Micromeritics (TriStar II 3020, Micromeritics Instrument Corporation, Norcross, GA, USA) instrument. The XRD analysis was carried out by a Philips PW 1729 (Philips, Amsterdam, Netherlands) X-ray diffractometer at room temperature using a $\text{Cu K}\alpha$ radiation operating at 40 kV and 30 mA to identify and confirm the crystalline phases. The size and surface elements of the as-modified catalysts were investigated using a TESCAN MIRA3 (TESCAN Brno, Brno-Kohoutovice, Czech Republic) field emission scanning electron microscope (FE-SEM) at an accelerating voltage of 15 kV coupled with an energy dispersive X-ray spectroscopy (EDS) detector. The X-ray photoelectron spectroscopy (XPS) examination was also performed on a Physical Electronics 5700 XPS instrument (PHI, Chanhassen, MN, USA) using a monochromatized $\text{Al K}\alpha$ radiation (1486.6 eV) operated at 350 W. Finally, diffuse reflectance spectra (DRS) were measured using an Avantes Avaspec-2048-TEC spectrometer (Avantes, Apeldoornseweg, Netherlands) with AvaLamp DH-S Setup which employed BaSO_4 as the reference.

3.3. Photocatalytic Experiments

Photocatalytic degradation of ethylbenzene in the air using the prepared N-doped P25 catalysts was evaluated at room temperature in an experimental annular reactor packed with glass beads on which the catalysts had been coated. To coat the catalysts on these supports, the surface of purchased glass beads with 5.5–6 mm diameter were physically roughened in a mixture of water, sandblasting sand and Carborundum powder using a mechanical mixer at 700 rpm for 20 min. They were also etched in 1 M NaOH solution for 5 min and then thoroughly washed with detergents and deionized water. Then the slurry with 2.5 g of N-doped TiO_2 powder in methanol/water mixture (95%/5%) was prepared having a 10 g/l concentration and completely dispersed by sonicating for 15 min. The coating of photocatalysts on the treated beads was performed by adsorption of the slurry on the heated glass beads ($100 \text{ }^\circ\text{C}$) and they were dried in an oven at $100 \text{ }^\circ\text{C}$. Finally, the coated glass beads were stabilized at $350 \text{ }^\circ\text{C}$ for 30 min [32,39]. The continuous gas flow photoreactor with the length of 40 cm was consisted of two coaxial tubes. The inner tube with an outer diameter of 42 mm was made of quartz glass housing the light source and the outer one was a Pyrex tube with 69 mm inner diameter packed with catalyst coated glass beads to a height of 27 cm which provided an effective volume of 230 mL in the reactor. The light source was a NARVA LT-T8 18 W (NARVA Lichtquellen GmbH, Brand-Erbisdorf, Germany) Freeze Light fluorescent lamp to investigate the photocatalytic activity under visible light and the UV irradiation was supplied by a Philips TUV T8 15 W SLV/25 (Philips Lighting, Eindhoven, Netherlands) germicidal lamp with a maximum emission at 254 nm to evaluate activity under UV

radiation. The Pyrex tube surface was covered with an aluminum foil to reflect the radiation into the reactor. The schematic diagram of the reaction system is shown in Figure 13.

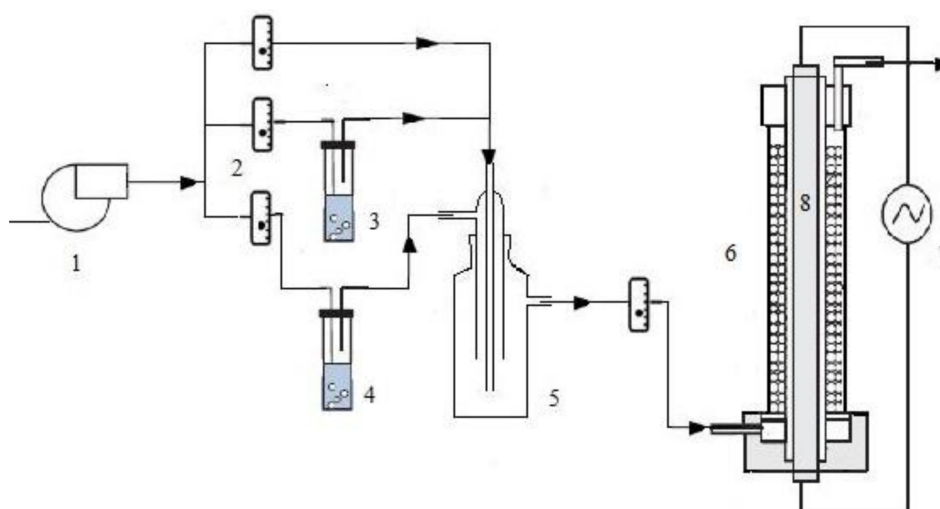


Figure 13. Schematics of the photocatalytic reaction system: (1) air pump, (2) rotameters, (3) humidifier, (4) ethylbenzene saturator, (5) mixing tank, (6) photoreactor, (7) power supply, (8) light source.

The reactor feed was prepared by mixing of ethylbenzene vapors and humid/dry air which were generated via passing the air through two glass impingers containing pure liquid ethylbenzene and distilled water. The air was supplied by an air pump (HAILEA, ACO-9620; Guangdong Hailea Group, Raoping, China) and was passed through activated carbon before entering the impingers. Ethylbenzene concentration and humidity were adjusted by rotameters controlling the air flow into the impingers and also the dry air entering the mixing tank. The concentration of ethylbenzene in the inlet and outlet streams of the photoreactor was measured by a TVOC fixed PID Detector (Ion Science Ltd, Royston, UK) and also the humidity and CO₂ content were measured by a SAMWON ENG SU-503B (Samwontech Co. Ltd, Bucheon, South Korea) device and a KIMO AQ-100 (KIMO Instruments, Chevry-Cossigny, France) CO₂ meter, respectively. The relative humidity was maintained around 50% in all experiments and each experiment was repeated three times with a reproducibility of better than 5%. The reactor inlet flow rate was adjusted by a rotameter just before entering the photoreactor. The feed flow was passed through the packed reactor before starting each catalytic experiment, in other words the light was turned on when the inlet and outlet ethylbenzene concentrations were equal and the flow stability was confirmed. The removal efficiency was measured after 30 min under UV experiments and after 90 min under visible light tests by observing steady state values. The removal efficiency of ethylbenzene is given by:

$$\text{Removal Efficiency (RE\%)} = (C_0 - C) \times 100 / C_0, \quad (2)$$

where C_0 is the inlet concentration of ethylbenzene and C is the outlet concentration. Moreover, a blank test was performed in the photoreactor packed with uncoated glass beads to investigate the photolysis effect and removal efficiency without photocatalyst in the reactor.

4. Conclusions

Application of nitrogen-doped commercial TiO₂ nano-catalysts for photocatalytic decomposition of ethylbenzene in the air using a packed-bed annular photoreactor in this study demonstrated that doping TiO₂ with nitrogen significantly enhanced photocatalytic conversion of ethylbenzene under visible light up to 60% in low initial concentrations compared with the use of pristine TiO₂, but such improvement under UV radiation was less than 5%. Also, the difference of photocatalytic activity between UV and visible light was considerable. The photocatalytic degradation under UV

irradiation could be achieved in much less residence times compared with the visible light and much higher initial ethylbenzene concentrations could be treated with appropriate removal efficiencies. For instance, the removal efficiency of ethylbenzene under UV irradiation using N-doped catalyst was more than 90% for the initial concentrations up to 0.586 g/m³ (135 ppmv) at 1 min residence time, but such removal efficiency under visible light radiation could be obtained for the initial concentrations up to 0.1 g/m³ (about 25 ppmv) at 3 min residence time. Moreover, the inlet flow rate and initial ethylbenzene concentration was effective on the removal efficiency under both UV and visible light. Increasing each of the initial ethylbenzene concentration and inlet flow rate resulted in reduction of removal efficiency. Furthermore, analyzing the kinetics of the photocatalytic reaction indicated that Langmuir-Hinshelwood kinetic model could be well fitted to the obtained experimental data under both UV and visible light irradiation. As for the obtained results under visible light irradiation and considering the N-doped TiO₂ nanoparticles which were prepared using a relatively facile and low-cost method, the photocatalytic reaction system in this research could be applied for the places with low pollutant concentration such as indoor air at homes to improve the air quality.

Author Contributions: Conceptualization, M.K. and H.R.; methodology, M.K. and S.M.M.D.; investigation and data analysis, M.K. and S.M.M.D.; writing—original draft preparation, M.K.; writing—review and editing, M.K., S.M.M.D and H.R.; supervision, S.M.M.D and S.T.; project administration, H.R.; funding acquisition, S.T.

Acknowledgments: The authors would like to acknowledge Research and Technology department of the National Iranian Oil Company (NIOC) for their financial support (Contract No. 71-92019).

Conflicts of Interest: The authors declare no conflicts of interest.

References

1. IEA. *World Energy Outlook Special Report 2016: Energy and Air Pollution*; International Energy Agency: Paris, France, 2016.
2. Mendola, P.; Wallace, M.; Liu, D.; Robledo, C.; Mannisto, T.; Grantz, K.L. Air pollution exposure and preeclampsia among US women with and without asthma. *Environ. Res.* **2016**, *148*, 248–255. [[CrossRef](#)] [[PubMed](#)]
3. Zhang, X.; Gao, B.; Creamer, A.E.; Cao, C.; Li, Y. Adsorption of VOCs onto engineered carbon materials: A review. *J. Hazard. Mater.* **2017**, *338*, 102–123. [[CrossRef](#)] [[PubMed](#)]
4. Kamal, M.S.; Razzak, S.A.; Hossain, M.M. Catalytic oxidation of volatile organic compounds (VOCs)—A review. *Atmos. Environ.* **2016**, *140*, 117–134. [[CrossRef](#)]
5. Masih, A.; Lall, A.S.; Taneja, A.; Singhvi, R. Exposure profiles, seasonal variation and health risk assessment of BTEX in indoor air of homes at different microenvironments of a terai province of northern India. *Chemosphere* **2017**, *176*, 8–17. [[CrossRef](#)] [[PubMed](#)]
6. Cheng, Z.-W.; Feng, L.; Chen, J.-M.; Yu, J.-M.; Jiang, Y.-F. Photocatalytic conversion of gaseous ethylbenzene on lanthanum-doped titanium dioxide nanotubes. *J. Hazard. Mater.* **2013**, *254–255*, 354–363. [[CrossRef](#)] [[PubMed](#)]
7. Ren, H.; Koshy, P.; Chen, W.-F.; Qi, S.; Sorrell, C.C. Photocatalytic materials and technologies for air purification. *J. Hazard. Mater.* **2017**, *325*, 340–366. [[CrossRef](#)] [[PubMed](#)]
8. Boyjoo, Y.; Sun, H.; Pareek, V.K.; Wang, S. A review on photocatalysis for air treatment: From catalyst development to reactor design. *Chem. Eng. J.* **2017**, *310*, 537–559. [[CrossRef](#)]
9. Graus, J.; Bueno-Alejo, C.J.; Hueso, J.L. In situ deposition of plasmonic gold nanotriangles and nanoprisms onto layered hydroxides for full-range photocatalytic response towards the selective reduction of p-nitrophenol. *Catalysts* **2018**, *8*, 354. [[CrossRef](#)]
10. Tasbihi, M.; Calin, I.; Suligoj, A.; Fanetti, M.; Lavrencic Stangar, U. Photocatalytic degradation of gaseous toluene by using TiO₂ nanoparticles immobilized on fiberglass cloth. *J. Photochem. Photobiol. A Chem.* **2017**, *336*, 89–97. [[CrossRef](#)]
11. Li, L.; Ma, Q.; Wang, S.; Song, S.; Li, B.; Guo, R.; Cheng, X.; Cheng, Q. Photocatalytic performance and degradation mechanism of aspirin by TiO₂ through response surface methodology. *Catalysts* **2018**, *8*, 118. [[CrossRef](#)]

12. Rengifo-Herrera, J.A.; Blanco, M.N.; Fidalgo de Cortalezzi, M.M.; Pizzio, L.R. Visible-light-absorbing Evonik P-25 nanoparticles modified with tungstophosphoric acid and their photocatalytic activity on different wavelengths. *Mater. Res. Bull.* **2016**, *83*, 360–368. [[CrossRef](#)]
13. Pham, T.-D.; Lee, B.-K. Selective removal of polar VOCs by novel photocatalytic activity of metals co-doped TiO₂/PU under visible light. *Chem. Eng. J.* **2017**, *307*, 63–73.
14. Foura, G.; Chouchou, N.; Soualah, A.; Kouachi, K.; Guidotti, M.; Robert, D. Fe-Doped TiO₂ supported on HY zeolite for solar photocatalytic treatment of dye pollutants. *Catalysts* **2017**, *7*, 344. [[CrossRef](#)]
15. Koltsakidou, A.; Antonopoulou, M.; Evgenidou, E.; Konstantinou, I.; Giannakas, A.E.; Papadaki, M.; Bikiaris, D.; Lambropoulou, D.A. Photocatalytic removal of fluorouracil using TiO₂-P25 and N/S doped TiO₂ catalysts: A kinetic and mechanistic study. *Sci. Total Environ.* **2017**, *578*, 257–267. [[CrossRef](#)] [[PubMed](#)]
16. Zhu, Z.; Murugananthan, M.; Gu, J.; Zhang, Y. Fabrication of a z-scheme g-C₃N₄/Fe-TiO₂ photocatalytic composite with enhanced photocatalytic activity under visible light irradiation. *Catalysts* **2018**, *8*, 112. [[CrossRef](#)]
17. Laciste, M.T.; de Luna, M.D.G.; Tolosa, N.C.; Lu, M.-C. Degradation of gaseous formaldehyde via visible light photocatalysis using multi-element doped titania nanoparticles. *Chemosphere* **2017**, *182*, 174–182. [[CrossRef](#)] [[PubMed](#)]
18. Zhang, L.; Tan, P.Y.; Lim, C.K.; Guo, X.; Tse, M.S.; Tan, O.K.; Chang, V.W. N-TiO₂-coated polyester filters for visible light photocatalytic removal of gaseous toluene under static and dynamic flow conditions. *J. Environ. Chem. Eng.* **2016**, *4*, 357–364. [[CrossRef](#)]
19. Huang, W.C.; Ting, J.-M. Novel nitrogen-doped anatase TiO₂ mesoporous bead photocatalysts for enhanced visible light response. *Ceram. Int.* **2017**, *43*, 9992–9997. [[CrossRef](#)]
20. Tryba, B.; Wozniak, M.; Zolnierkiewicz, G.; Guskos, N.; Morawski, A.; Colbeau-Justin, C.; Wrobel, R.; Nitta, A.; Ohtani, B. Influence of an electronic structure of N-TiO₂ on its photocatalytic activity towards decomposition of acetaldehyde under UV and fluorescent lamps irradiation. *Catalysts* **2018**, *8*, 85. [[CrossRef](#)]
21. Khalilzadeh, A.; Fatemi, S. Spouted bed reactor for VOC removal by modified nano-TiO₂ photocatalytic particles. *Chem. Eng. Res. Des.* **2016**, *115*, 241–250. [[CrossRef](#)]
22. Ochiai, T.; Fujishima, A. Photoelectrochemical properties of TiO₂ photocatalyst and its applications for environmental purification. *J. Photochem. Photobiol. C Photochem. Rev.* **2012**, *13*, 247–262. [[CrossRef](#)]
23. Ibhaddon, A.O.; Fitzpatrick, P. Heterogeneous photocatalysis: Recent advances and applications. *Catalysts* **2013**, *3*, 189–218. [[CrossRef](#)]
24. Ida, J.; Watanabe, T.; Watanabe, S.; Matsuyama, T.; Yamamoto, H. Photocatalytic packed bed reactor design for efficient UV light use. *Sep. Purif. Technol.* **2014**, *134*, 66–72. [[CrossRef](#)]
25. Wang, T.; Li, W.; Xu, D.; Wu, X.; Cao, L.; Meng, J. Strong visible absorption and excellent photocatalytic performance of brown TiO₂ nanoparticles synthesized using one-step low-temperature process. *Chin. J. Catal.* **2017**, *38*, 1184–1195. [[CrossRef](#)]
26. Le, T.K.; Flahaut, D.; Martinez, H.; Hung Nguyen, H.K.; Xuan Huynh, T.K. Study of the effects of surface modification by thermal shock method on photocatalytic activity of TiO₂ P25. *Appl. Catal. B* **2015**, *165*, 260–268.
27. Ohtani, B.; Prieto-Mahaney, O.O.; Li, D.; Abe, R. What is Degussa (Evonik) P25? Crystalline composition analysis, reconstruction from isolated pure particles and photocatalytic activity test. *J. Photochem. Photobiol. A Chem.* **2010**, *216*, 179–182. [[CrossRef](#)]
28. Nawawi, W.I.; Nawi, M.A. Carbon coated nitrogen doped P25 for the photocatalytic removal of organic pollutants under solar and low energy visible light irradiations. *J. Mol. Catal. A Chem.* **2014**, *383–384*, 83–93. [[CrossRef](#)]
29. Rengifo-Herrera, J.A.; Kiwi, J.; Pulgarin, C. N, S co-doped and N-doped Degussa P-25 powders with visible light response prepared by mechanical mixing of thiourea and urea. Reactivity towards *E. coli* inactivation and phenol oxidation. *J. Photochem. Photobiol. A Chem.* **2009**, *205*, 109–115. [[CrossRef](#)]
30. Anovitz, L.M.; Cole, D.R. Characterization and analysis of porosity and pore structures. *Rev. Mineral. Geochem.* **2015**, *80*, 61–164. [[CrossRef](#)]
31. Jin, Z.; Duan, W.; Duan, W.; Liu, B.; Chen, X.; Yang, F.; Guo, J. Indium doped and carbon modified P25 nanocomposites with high visible-light sensitivity for the photocatalytic degradation of organic dyes. *Appl. Catal. A* **2016**, *517*, 129–140. [[CrossRef](#)]

32. Khalilian, H.; Behpour, M.; Atouf, V.; Hosseini, S.N. Immobilization of S, N-codoped TiO₂ nanoparticles on glass beads for photocatalytic degradation of methyl orange by fixed bed photoreactor under visible and sunlight irradiation. *Sol. Energy* **2015**, *112*, 239–245. [[CrossRef](#)]
33. Bakar, S.A.; Ribeiro, C. Low temperature synthesis of N-doped TiO₂ with rice-like morphology through peroxy assisted hydrothermal route: Materials characterization and photocatalytic properties. *Appl. Surf. Sci.* **2016**, *337*, 121–133. [[CrossRef](#)]
34. Pu, X.; Hu, Y.; Cui, S.; Cheng, L. Preparation of N-doped and oxygen-deficient TiO₂ microspheres via a novel electron beam-assisted method. *Solid State Sci.* **2017**, *70*, 66–73. [[CrossRef](#)]
35. Youssef, L.; Kinfaek Leoga, A.J.; Roualdes, S.; Bassil, J.; Zakhour, M.; Rouessac, V.; Ayrat, A.; Nakhil, M. Optimization of N-doped TiO₂ multifunctional thin layers by low frequency PECVD process. *J. Eur. Ceram. Soc.* **2017**, *37*, 5289–5303. [[CrossRef](#)]
36. Jeon, J.-W.; Lee, D.-H.; Won, Y.S.; Lee, M.-G. Characteristics of photocatalytic decomposition of individual and binary mixture vapors of some VOCs by a cylindrical UV reactor with helically installed TiO₂-coated perforated planes. *Korean J. Chem. Eng.* **2018**, *35*, 744–749. [[CrossRef](#)]
37. Chun, H.-H.; Jo, W.-K. Visible-light-responsive carbon-embedded photocatalyst coupled with plug-flow reactor for decomposition of vaporous aromatics. *Chin. J. Catal.* **2013**, *34*, 1256–1261. [[CrossRef](#)]
38. Hinojosa-Reyes, M.; Arriaga, S.; Diaz-Torres, L.A.; Rodríguez-González, V. Gas-phase photocatalytic decomposition of ethylbenzene over perlite granules coated with indium doped TiO₂. *Chem. Eng. J.* **2013**, *224*, 106–113. [[CrossRef](#)]
39. Korologos, C.A.; Nikolaki, M.D.; Zerva, C.N.; Philippopoulos, C.J.; Pouloupoulos, S.G. Photocatalytic oxidation of benzene, toluene, ethylbenzene and m-xylene in the gas-phase over TiO₂-based catalysts. *J. Photochem. Photobiol. A Chem.* **2012**, *244*, 24–31. [[CrossRef](#)]



© 2018 by the authors. Licensee MDPI, Basel, Switzerland. This article is an open access article distributed under the terms and conditions of the Creative Commons Attribution (CC BY) license (<http://creativecommons.org/licenses/by/4.0/>).